# A Comprehensive Investigation on the Enhancing the Thermal Efficiency of Solid Oxide Fuel Cells through Temperature and Pore Diameter Optimization

Berre KÜMÜK<sup>a</sup>, Nisa Nur ATAK<sup>b</sup>, Battal DOĞAN<sup>c</sup>, Murat Kadir YEŞİLYURT<sup>d,\*</sup>

<sup>a</sup> Automotive Technologies Program, Motor Vehicles and Transportation Technologies Department, Iskenderun Vocational School of Higher Education, Iskenderun Technical University, Hatay, Türkiye

\* Corresponding author

E-mail address: kadir.yesilyurt@bozok.edu.tr (MK Yesilyurt)

## **ABSTRACT**

This study aims to comprehensively analyze the performance of solid oxide fuel cells (SOFCs) operating at high temperatures and converting chemical energy directly into electrical energy, considering the effects of multiple parameters. The cell performance was evaluated in the analysis performed on a cell with an active surface area of 0.01 m², a temperature range of 573–1673 K and pore diameters of 3–15  $\mu m$ . The performance evaluation involved a meticulous examination of activation, ohmic, and concentration losses, along with the determination of cell potential, power density, and thermal efficiency through theoretical analyses. The findings showed that the temperature increase positively affected the cell efficiency up to a certain threshold; it was determined that the thermal efficiency reached its peak especially in the temperature range of 1073 - 1273 K. A 20% efficiency increase was achieved under the conditions of a temperature increase of 210 K, a current density of 10000 A/m² and a pore diameter of 8  $\mu m$ . While 33.04% and 21.41% efficiency values were obtained with 5  $\mu m$  and 10  $\mu m$  pore diameters, respectively, at a constant temperature of 873 K, a 60% increase in pore

<sup>&</sup>lt;sup>b</sup> Gazi University Institute of Science, Gazi University, Ankara, Türkiye

<sup>&</sup>lt;sup>c</sup> Department of Energy Systems Engineering, Faculty of Technology, Gazi University, Ankara, Türkiye

<sup>&</sup>lt;sup>d</sup> Department of Mechanical Engineering, Faculty of Engineering-Architecture, Yozgat Bozok University, Yozgat, Türkiye

diameter provided only an 8% efficiency increase, which revealed that the increase in pore diameter had limited and negative effects on efficiency. Unlike the generally single parameter focused cases in the literature, this research demonstrates conclusively that the length of the width diameter will lead to a noticeable decrease in thermal efficiency by providing a joint analysis of multiple variables in the cell.

**Keywords:** Solid oxide fuel cell; operating temperature; pore diameter; theoretical analysis; thermal efficiency



## 1. INTRODUCTION

The current energy needs and environmental concerns have accelerated the development for sustainable energy production. The use of renewable energy source will contribute to a decrease in environmental concerns and energy costs. The most significant challenge remains in the initial investment costs for the utilization of renewable energy sources, which have not yet seen sufficient reduction. In recent years, hydrogen production from renewable sources has attracted the attention of many researchers. Studies, especially those focusing on the production of green hydrogen through the electrolysis of water using electricity generated from renewable energy sources, have gained momentum. Fuel cells are used for electricity generation from hydrogen, with proton exchange membrane (PEM) fuel cells at low operating temperatures and solid oxide fuel cells (SOFC) at high operating temperatures being the preferred options in today's context.

In this context, solid oxide fuel cells have gained significant attention as energy conversion technologies. Solid oxide fuel cells are highly efficient, have low environmental impact, and are flexible in utilizing various fuel options [1]. The thermodynamic foundations of this technology are critical for understanding and optimizing the system performance [2]. Solid oxide fuel cells represent a crucial step towards an energy-efficient and environmentally friendly future [3–5].

A literature review reveals experimental and numerical studies on the performance of solid oxide fuel cells (SOFC). Wang et al. [6] conducted a study using a one-dimensional mathematical model to calculate the distributions of the key parameters in an adiabatic environment with different inlet gas temperatures and current densities. The results indicated that the optimal inlet gas temperature for SOFC operating in an adiabatic environment varied between 873 K and 973 K when the average current density ranged from 0.05 A cm<sup>-2</sup> to 0.25 A cm<sup>-2</sup>. Furthermore, when studying the counterflow and co-flow situations, it was observed that the output power of the counterflow SOFC was approximately 11.3% higher than that of the co-flow SOFC within the investigated range. Sahli et al. [7] performed a thermodynamic analysis, examining the Nernst potential arising from concentration, activation, and ohmic polarization using the FORTRAN program code. According to the results, the cell potential and power density were proportional to changes in the operating temperature and oxygen concentration in the oxidant. Conversely, the feed pressure changes, fuel humidity, and electrolyte thickness exhibited an inverse relationship. Cao et al. [8] investigated the role of changes in the nitrogen ratio along with two main fuel cell design parameters: the current

density and fuel utilization factor. They also compared the thermodynamic, economic, and environmental performance of two different electrolytes under the same conditions. The results indicated that as the input nitrogen ratio increased, the voltage output of each cell, as well as the energy and exergy efficiencies, electricity generation rate, and exergoeconomic factor of the applications decreased. Meanwhile, the unit electricity cost and carbon dioxide emissions increased. Additionally, the sensitivity to a performance decrease was found to be higher for nitrogen ratios above 0.7.

Solid oxide fuel cells (SOFCs) have a significant advantage over other fuel cells because of their high operating temperature, which allows the use of alternative fuels. The use of different fuel types in fuel cells can provide additional options for industrial applications. The performance and losses of various alternative fuels in thermodynamic analyses can be evaluated, enabling comparisons of their advantages and disadvantages compared to hydrogenfueled solid oxide fuel cells [9–14]. Another important advantage of oxide fuel cells is that they produce exhaust gases at high temperatures, allowing integration with different systems to enhance the overall system performance and efficiency. There are various studies in the literature that include thermodynamic analyses of systems created in this manner. Sinha et al. [15] investigated the combined use of a gas turbine and solid oxide fuel cells (SOFC). Wood chips were used as the gasifier feedstock, and the synthesis gas produced as a byproduct was processed and used in fuel cells. Irreversibility in the system leads to exergy destruction and, increase losses associated with the components. The maximum exergy destruction includes the SOFC, water heat exchanger, and gasifier. The maximum thermal efficiency of the implemented hybrid system was found to be 62.12% at a pressure ratio of 4 and temperature of 1250 K. Ryu et al. [16] established a combined SOFC (Solid Oxide Fuel Cell) - Gas Turbine (GT) system to generate power in marine propulsion facilities. This system was designed and modeled using Aspen HYSYS V.12.1. The thermodynamic performance of the system was analyzed using the first and second laws of thermodynamics. The energy efficiencies of direct ammonia and hydrogen SOFCs were found to be 60.96% and 64.46%, respectively. The energy efficiencies of the combined systems increased by 12.37% and 13.97% compared to the standalone SOFC systems when ammonia and hydrogen as fuels. The study also examined the exergy destruction of the essential components for each fuel and conducted a parametric study to select the optimal fuel utilization factor for the system. The analysis demonstrated the potential of ammonia as a hydrogen carrier and the effective use of waste heat recovery to enhance the thermodynamic performance of SOFC systems. Trujillo et al. [17] presented a comparative

assessment of a combined molten carbonate fuel cell and solid oxide fuel cell stack with a micro gas turbine. The components of the system were sized using the first law of thermodynamics to satisfy the thermal conditions required for the operation of the fuel cell stack. An exergetic analysis was also performed to evaluate the reversibility of the components. The results showed that MCFC stacks were more efficient than SOFC stacks but were significantly more expensive. Alirahmi et al. [18] proposed a new storage configuration for electricity production by combining a solid oxide fuel cell, compressed air energy storage, and a brine desalination unit. An analysis of the economic, environmental, and thermodynamic performances of the system was conducted. The exergy efficiency of the proposed system was determined to be 71.03%, with a total cost of \$34.07 per hour and pollution rate of 0.184 kg/kWh. Pirkandi et al. [19] analyzed the thermodynamic performance of a hybrid system consisting of a steam turbine, gas turbine, and solid oxide fuel cell. This hybrid system stands out from other existing cycles because it involves the simultaneous use of three modern technologies in the same power generation cycle. The study initially examined nine different steam cycle configurations and, selects the best cycle based on the thermodynamic performance. The results indicated that the triple hybrid cycle, which includes the addition of a steam cycle to a gas turbine-fuel cell combined cycle, increased the net power produced by the triple system by 200% compared to a simple gas turbine cycle and by 15% compared to a gas turbine-fuel cell hybrid cycle. The results also showed that the triple hybrid system with 52% efficiency outperformed the gas turbine-fuel cell hybrid system with a 45.21% efficiency and the simple gas turbine cycle with 25% efficiency.

The losses occurring in solid oxide fuel cells and the significant impact of different operating conditions on the performance of solid oxide fuel cells are well-known [20–25]. Studies have shown that-the performance of solid oxide fuel cells generally increases with the temperature and pressure [26–30]. Additionally, there are studies in the literature that investigate the effects of increasing pore size on performance [31–33].

In recent years, there are studies in the literature focusing on minimizing entropy production, waste heat recovery and industrial optimization strategies in order to increase the efficiency of SOFC systems [34–44].

In this article, the authors focus on the thermodynamic principles of oxide fuel cells to understand the fundamental principles and potential applications of this innovative energy conversion technology. Studies in the literature have calculated the current density, losses, and

power density of fuel cells within specific temperature ranges. In this study, the performance of the fuel cell was evaluated in the temperature range of 573 K to 1673 K. Losses will be calculated based on different pore sizes, thereby determining the thermal efficiency under optimal operating conditions.

## 2. MATERIALS and METHODS

Fuel cells are electrochemical devices that are capable of directly producing electrical energy through chemical reactions. Fuel cells can be classified based on three fundamental criteria: operating temperature, electrolyte type, and type of hydrogen source used. Solid oxide tuel cell (SOFC) operate at high temperatures. This type of fuel cell generates electrical energy through electrochemical reactions between oxygen and the fuel mediated by a solid oxide electrolyte. As shown in Figure 1, the basic components of oxide fuel cells are the anode, cathode, and electrolyte. The fundamental operating principle can be expressed as the separation of fuel at the anode and oxygen at the cathode. Oxygen ions on the cathode side migrate through the electrolyte to interact with the fuel; such as oxidized hydrogen, methane, biogas, or hydrocarbons [45]. As a result of this interaction, electrons are released, and electrical energy is generated. During the operation of the system, by products, such as water or carbon dioxide, are formed.

The chemical reactions occurring at the anode and cathode are described below. The reaction between hydrogen and oxygen leads to water formation. The energy released during this reaction generates electricity at the electrodes.

Anode: 
$$2H_2 + 2O_2 \rightarrow 2H_2O + 4e^-$$
 (1)

Cathode: 
$$O_2 + 4e^- \rightarrow 2O^{-2}$$
 (2)

Overall cell reaction: 
$$H_2 + 1/2O_2 \rightarrow H_2O + 2e^-$$
 (3)

The cell potential (V) of a solid oxide fuel cell is determined by subtracting all activation losses  $(\eta_{act})$ , concentration losses  $(\eta_{conc})$ , and ohmic losses  $(\eta_{ohmic})$ , occurring in the anode and cathode regions during the electricity generation process from the equilibrium potential (E) of the cell. The cell potential is obtained by considering these losses and is used to evaluate the operating conditions of the solid oxide fuel cell in comparison to the equilibrium potential.

$$V = E - \eta_{act,a} - \eta_{act,c} - \eta_{conc,a} - \eta_{conc,c} - \eta_{ohmic}$$

$$\tag{4}$$

A cell's equilibrium potential (E) signifies the state in which the electrochemical reactions are at equilibrium. When the cell reaches equilibrium potential, the chemical reactions and electron flow are in a balanced state. In this situation, no net current was generated in the electrochemical cell reactions, indicating that the cell had a constant electric potential. The equilibrium potential (E) was calculated using the Nernst equation (Eq. 5. where  $E_0$  is the reversible potential, R is the universal gas constant, F is the Faraday constant, and  $P_{H_2}$ ,  $P_{H_2O}$ ,  $P_{O_2}$  represent the pressures of hydrogen, oxygen, and water, respectively.

$$E = E_0 + \frac{RT}{2F} \ln \left( \frac{P_{H_2} P_{O_2}^{1/2}}{P_{H_2O}} \right)$$

The reversible potential  $(E_0)$  was calculated based on temperature (T) and represented a standard condition [46].

$$E_0 = 1.253 - 2.4516x10^{-4}T \tag{6}$$

To explain the activation polarization losses  $(\eta_{act})$  occurring in electrochemical reactions within the fuel cell, the Butler-Volmer equation was utilized. The equation is, given in Eq. 7, varies with the current density (J), exchange current densities at the anode and cathode  $(J_{0,a}, J_{0,c})$ , number of electrons (z=2), and the symmetry factor  $(\alpha=0.5)$  [47].

$$J = J_0 \left[ \exp\left(\frac{\alpha z F \eta_{act}}{RT}\right) - \exp\left(\frac{(1-\alpha)z F \eta_{act}}{RT}\right) \right]$$
 (7)

Activation losses in solid oxide fuel cells are a determining factor for the rate of chemical reactions that occur on the electrode surface. The activation losses are calculated as part of the Butler-Volmer equation, as shown below. This equation determines the anode  $(\eta_{act,a})$  and

cathode ( $\eta_{act,c}$ ) activation losses based on cell temperature (T), current density, and exchange current density [48].

$$\eta_{act,a} = \frac{RT}{F} \sinh^{-1} \left( \frac{J}{2J_{0,a}} \right) \tag{8}$$

$$\eta_{act,c} = \frac{RT}{F} \sinh^{-1} \left( \frac{J}{2J_{0,c}} \right) \tag{9}$$

The exchange current density is denoted as  $J_0$  and can be calculated in two different forms for the anode and cathode.  $J_0$  is influenced by pore diameter  $(D_p)$ , particle size  $(D_s)$ , electrode porosity (n), and pressure (P) [47]. The values of these parameters are listed in Table 1.

$$J_{0,a} = k_a \frac{72 \times \left[D_p - \left(D_p + D_s\right)n\right]n}{D_s^2 D_p^2 \left(1 - \sqrt{1 - X^2}\right)} \times \left(\frac{P_{H_2}}{P_{ref}}\right) \left(\frac{P_{H_2O}}{P_{ref}}\right) \exp\left(\frac{E_{act,a}}{RT}\right)$$
(10)

$$J_{0,c} = k_c \frac{72 \times \left[ D_p - \left( D_p + D_s \right) n \right] n}{D_s^2 D_p^2 \left( 1 - \sqrt{1 - \alpha^2} \right)} \times \left( P_{o_2} \right)^{0.25} \exp \left( -\frac{E_{act,c}}{RT} \right)$$
(11)

Concentration losses  $(\eta_{colc})$  in an SOFC refer to energy loss stemming from variations in the concentration of reactants or products at the anode and cathode. These losses occur during the diffusion of gases onto the electrode surface, which is typically explained by Fick's law of diffusion. This law elucidates how gases diffuse along the electrode surface and how this diffusion affects the cell performance. Concentration losses at the anode and cathode were calculated as follows: [46, 49, 50]:

$$\eta_{conc,a} = \frac{RT}{2F} \ln \left[ \frac{1 + \frac{RTd_a J}{2FD_a^{eff} P_{H_2O}^0}}{1 - \frac{RTd_a J}{2FD_a^{eff} P_{H_2}^0}} \right]$$
(12)

$$\eta_{conc,c} = \frac{RT}{2F} \ln \left[ \frac{1}{1 - J/J_{L,O_2}} \right] \tag{13}$$

For oxygen, the limiting current density  $(J_L)$  can be determined using Eq. 14, where it is dependent on the number of electrons (z), cathode effective gas diffusion factor  $(D_c^{\it eff})$ , cathode electrode thickness  $(d_c)$ , and partial pressure of  $O_2(p_{o_2})$  [51]:

$$J_{L,O_2} = \frac{zFD_c^{eff}}{RTd_c} p_{O_2}$$

$$\tag{14}$$

The effective gas-diffusion factors at the anode and cathode ( $D_a^{eff}$ ,  $D_c^{eff}$ ) were calculated using the Knudsen diffusion coefficient. Where  $\xi$  represents the anode-cathode curvature, and n represents the anode-cathode porosity [46].

$$\frac{1}{D_a^{eff}} = \frac{\xi}{n} \left( \frac{1}{D_{H_2 - H_2 O}} + \frac{1}{D_{H_2, k}} \right) \tag{15}$$

$$\frac{1}{D_c^{eff}} = \frac{\xi}{n} \left( \frac{1}{D_{O_2 - N_2}} + \frac{1}{D_{O_2, k}} \right) \tag{16}$$

The binary diffusion coefficient of  $O_2$  in an  $O_2$ - $N_2$  air mixture is denoted as  $D_{O_2-N_2}$ . The diffusion gas volume (v) for the selected gas type, fuel cell temperature (T), and reference pressure  $(P_{ref})$  are included in Fuller's diffusion equation [52].

$$D_{O_2-N_2} = \frac{0.00143T^{1.75}}{M_{O_2-N_2}^{1/2} \left(v_{O_2}^{1/3} + v_{N_2}^{1/3}\right)^2 P}$$
(17)

The expression for  $M_{O_2-N_2}$  given in Eq. 18 is calculated as follows, depending on the molecular weights of oxygen gas  $M_{O_2}$  and nitrogen gas  $M_{N_2}$ :

$$M_{O_2-N_2} = 2\left(\frac{1}{M_{O_2}} + \frac{1}{M_{N_2}}\right)^{-1}$$
 (18)

The diffusion coefficient expressed by Knudsen for  $O_2$  in an air mixture was determined according to Eq. 19. This value varies depending on the pore diameter  $(D_p)$ , cell temperature (T), and molecular weight of the gas  $(M_{H_2})$  [46].

$$D_{O_2,k} = 97 D_p \sqrt{\frac{T}{M_{H_2}}} \tag{19}$$

Ohmic losses in SOFC are energy losses that occur owing to the resistance of the electric current. These losses arise depending on factors such as the electrolyte thickness (L), cell temperature (T), and current density (J) in the fuel cell, as given below [53].

$$\eta_{ohmic} = 2.99 \times 10^{-11} J L exp \left( \frac{10300}{T} \right)$$
(20)

Thermal efficiency is an important parameter for assessing the performance of fuel cells. In a solid oxide fuel cell, the thermal efficiency represents the ratio of the power density obtained from electrochemical reactions in the cell to the energy taken from the fuel. Mathematically, it can be defined as:

$$\eta_{thermal} = \frac{Power Density}{Fuel Energy} \tag{21}$$

# 3. RESULTS AND DISCUSSIONS

This study was conducted to evaluate the performance of solid oxide fuel cells at different temperatures (573-1673 K) and pore sizes (3  $\mu$ m, 5  $\mu$ m, 8  $\mu$ m, 10  $\mu$ m, 15  $\mu$ m). The activation, ohmic, and concentration losses affecting SOFC performance were calculated under various operating conditions. In additionally, power density and thermal efficiency were determined. These calculations are crucial for optimizing the performance of a solid oxide fuel cell operating under various conditions.

The activation losses in the cell were calculated for different operating temperatures while maintaining the pore size of the SOFC constant at 3 µm, as shown in Fig. 2. The variation in operating temperature has a significant impact on the activation losses at the cathode and anode. As seen in Eqs. 10 and 11, an increase in the operating temperature led to an increase in the exchange current density. Because the temperature change is exponential in these equations, any increase or decrease in the temperature results in a noticeable change in the exchange current density. Eq. 7 expresses the influence of the exchange current density and temperature on activation losses. Because the substantial effect of temperature change on the exchange current density, activation losses are highly affected.

This phenomenon occurred because a decrease in temperature led to a reduction in the exchange current density, causing the chemical reactions to proceed more slowly. The minimum activation loss in the cell was calculated as 0.01264 V at 1373 K. At a constant current density of 20,000 A/m², the total activation loss of the cell was 0.3874 V at a working temperature of 1173 K and, 2.4835 V at 573 K. As the current density in the fuel cell increase d, the activation losses also increased. With an increase in the current density from 2500 A/m² to 17500 A/m² at a cell temperature of 973 K, the total activation loss of the cell was 0.3913 V and 0.9907 V, respectively. In a study conducted by Chan et al. [46], calculations were performed on various parameters in solid oxide fuel cells (SOFCs), whether anode-supported or cathode-supported. An increase in current density increased the activation losses in the cell. At an operating temperature of 1073 K, a 50% increase in the current density increased the total activation loss in both the anode and cathode by 33.3%.

The change in activation losses with temperature variation in the range of 1273-1673 K is provided in Table 2. When the temperature is increased from 1273 K to 1573 K, activation losses at a current density of 2500 A/m² decrease by approximately 83%. Upon raising the operating temperature from 1573 K to 1673 K the activation losses are decreased by 36.58%. Increasing the operating temperature from 1273 K to 1373 K decreased the activation losses by approximately 50%. Similarly, increasing the temperature from 1373 K to 1473 K leads to a decrease of approximately 45% in the activation losses. Under high-temperature operating conditions, the rate of concentration loss reduction diminishes with every 100 K increase. Activation losses play a significant role in material selection, particularly under high-temperature operating conditions in Solid Oxide Fuel Cells (SOFCs). Chan et al. [54] conducted

a performance analysis of an SOFC with an active surface area of 0.027 m², anode and cathode thicknesses of 0.00015 and 0.002 m, respectively, under various operating temperatures and pressures. The study revealed a pronounced contrast between the temperature and activation losses. The highest losses were observed at the lowest operating temperatures. For instance, increasing the operating temperature by 200 K at a current density of 75 mA/cm² resulted in an approximate 0.14 V increase in activation loss.

The SOFC pore size represents the number of voids present in the internal structure of the material within the cell. These pores are critical areas that influence the movement of gases and reactants within a material. Changes in the pore size significantly affected the gas transfer and reaction kinetics of the cell. An increase in pore size noticeably reduced the exchange current density. For example, the variation in current density at a pore size of 3  $\mu$ m is 19.43%, 42.4%, and 52% higher than that at pore sizes of 5  $\mu$ m, 8  $\mu$ m, and 10  $\mu$ m, respectively. As seen in Figure 3, an increase in the pore size of a solid oxide fuel cell leads to an increase in activation losses. Additionally, larger pores increase the time required for gas molecules to reach the electrode surface, making gas diffusion more challenging.

The largest activation loss in the cell was observed at a pore size of 15  $\mu$ m, amounting to 1.075 V. At a constant current density of 10,000 A/m², the activation loss is 0.52 V for a pore size of 5  $\mu$ m, while it increases to 0.70 V with a pore size of 10  $\mu$ m. A 50% increase in the pore size of the fuel cell results in a 0.126 V increase in activation losses. Ni et al. [47] investigated the impact of the operating temperature and pore size on the performance of SOFC at varying current densities. The study includes a comparison between the experimental data and modeled fuel cells. An increase in pore size has a significant effect on concentration losses, leading to a 0.18 V increase in concentration loss when the pore radius increases from 3  $\mu$ m to 10  $\mu$ m.

The impact of the temperature variation on the concentration losses is shown in Figure 4. The limiting current density significantly influences the concentration losses in SOFCs. As the temperature increased, the limiting current density decreases noticeably. When the temperature increased from 873 to 1273 K, the limiting current density decreased by 43.23%. The concentration losses in the fuel cell, at a constant current density were, 0.0542 V when the operating temperature was 673 K and increased to 0.1885 V at an operating temperature of

1173 K. Unlike activation losses, concentration losses increase with increase in temperature, as showen in Eq. 12, where R and F are constants, making the temperature change more pronounced compared to the logarithmic expression. Additionally, because pressure changes do not have a significant impact on SOFC performance, the concentration losses are predominantly affected by temperature. Ni et al. [47] calculated the cell losses, voltage, and power density of a high-temperature SOFC under varying parameters and compared the experimental and model data. The comparison values showed similar similarities. Moreover, an increase in operating temperature also increased the concentration loss. At a constant current density of 15,000 A/m², the concentration loss at 873 K is 0.1 V, whereas it is 0.2 V at a temperature of 1273 K.

In Figure 5, the variation of cell potential with current density for SOFC with a constant pore size at different temperatures is presented. A decrease in the temperature of the fuel cell results in a reduction in the cell voltage. This is attributed to the fact that lower temperatures increase the cell loss. The increase in losses leads to deductions from the equilibrium potential of the cell, as indicated in Equation 4, thereby causing a decrease in the cell voltage. While the cell potential tends to increase with temperature in solid oxide fuel cells, the impact of this increase on the cell efficiency diminishes after a certain temperature. Therefore, in solid oxide fuel cells operating at either low (T < 873 K) or high temperatures (T > 1273 K), the cell potential does not reach the desired levels. Designs and improvements that reduce activation losses are needed for SOFCs operating at high or low temperatures. Additionally, low temperatures struggle to provide the energy necessary for the initiation of chemical reactions, further lowering the cell voltage.

With a current density of 10,000 A/m², increasing the operating temperature from 973 to 1373 K resulted in a 71.55% increase in the cell potential. For a constant operating temperature in a solid øxide fuel cell (1173 K), the cell voltage was 0.9219 V at a current density of 5000 A/m², which decreased to 0.6250 V at a current density of 15,000 A/m². Singhal [55] compared the theoretical and actual operational performances of SOFC under various operating parameters such as temperature and pressure. Although the cell potential increases with temperature, an increase in the current density has a negative effect on the potential. At a constant operating temperature of 900 °C, a 200 mA/cm² increase in the current density reduces the voltage by 0.28 V. Furthermore, current density250 mA/cm², a 25% increase in temperature results in a 0.36 V increase in voltage.

Lin et al. [56] extensively examined important parameters such as the cell voltage and cell flow rate of an SOFC with 20 cells under various operating conditions. At a current density of 5000 A/m², the cell potential is 0.79 V, 0.7 V, and 0.5 V at operating temperatures of 850 °C, 800 °C, and 750 °C, respectively. While an increase in the current density reduces the cell voltage, an increase in temperature elevates the voltage.

Figure 6 illustrates the impact of pore size on the cell potential in the SOFC. An increase in the pore size of the fuel cell negatively affects the exchange current density, leading to an increase in activation losses. This increase in activation losses results in a decrease in cell potential. In addition, the larger pores restrict gas diffusion. At a constant current density of 12,500 A/m², the cell voltages for pore sizes of 5  $\mu$ m and 10  $\mu$ m were 0.3978 and/0.2189 V, respectively. The maximum cell potential value was calculated as 0.9348 V for a 3  $\mu$ m pore size in a solid oxide fuel cell at an exchange current density of 2500 A/m².

In this study, at a constant current density, increasing the pore size threefold led to a 36.78% increase in the fuel cell voltage. For an 8 µm pore size in the SOFC fuel cell, the cell potential was 0.8395~V at  $2500~A/m^2$  and a current density of 0.6431~V at  $5000~A/m^2$  current density. This indicates that an increase in the current density resulted in a decrease in the cell voltage. In their study, Ni et al. [47] calculated the concentration, ohmic, and activation losses, cell potential, and power density of SOFC at three different operating temperatures and five different pore sizes. The cell potential was highest in cells with a small pore size. Increasing the pore size from 3 µm to  $10~\mu m$  resulted in a 33.3% voltage loss.

The primary goal of SOFCs is to maximize cell voltage by minimizing losses. If the activation and ohmic losses increase exessively owing to the high operating temperatures, it adversely affects the voltage. Figures 7 and 8 illustrate the variation in the power density obtained at different current densities with the temperature and pore size. For a current density of 5000 A/m² in a solid oxide fuel cell, the power density at a cell temperature of 1173 K was 4609.63 W/m², whereas it decreased to 640.886 W/m² at 873 K. The maximum power density was achieved at a working temperature of 1373 K and current density of 20,000 A/m², with a value of 13696.1 W/m². A decrease in the operating temperature below 873 K adversely affects the

performance of the solid oxide fuel cell. Tsai and Barnett [57] conducted detailed calculations of cell losses, cell voltages, and power densities for SOFC with various electrolyte thicknesses, material porosities, and operating temperatures. The study reveals that every 50 °C increase in temperature leads to an approximately 0.20 V increase in cell voltage.

Chan et al. [46] performed performance analyses on an anode or electrolyte-supported SOFC under a constant operating temperature of 1073 K and 1 atm pressure. In this study, the power density of an anode-supported SOFC with a thickness of 750 µm is calculated at various current densities. Power density initially increased and then decreased with increasing current density, exhibiting a parabolic trend. The maximum power density was calculated at 12,000 A/m² current density, reaching 5100 W/m².

An increase in the pore size of SOFC leads to cell losses, resulting in a low power density. A 70% increase in the pore size of the fuel cell leads to a decrease in power density of 2391.55 W/m². In this study, doubling the current density with a pore size of 5  $\mu$ m resulted in a 24% increase in power density. For a constant current density of 15,000 A/m² in the fuel cell, the power density was 2996.03 W/m² with an 8  $\mu$ m pore size, whereas it dropped to 103.14 W/m² with a pore size of 15  $\mu$ m. The fuel cell performed significantly better with smaller pore sizes. Studies in the literature also show that an increase in pore size negatively affects power density, with a 1.5-fold increase in pore size leading to a 44.4% decrease [47].

In fuel cells, thermal efficiency is calculated in accordance with the first law of thermodynamics. This represents the useful work obtained from the fuel cell as power density. The primary goal of a fuel cell is to achieve the highest voltage at a specific current density to achieve the maximum power density. The energy expended to achieve this power density is part of the denominator of thermal efficiency. The thermal efficiency is directly proportional to the increase in the power density. To increase power density, it is crucial to reduce ohmic, concentration, and activation losses. Any measure taken to reduce these losses will positively impact the thermal efficiency. The increase in power density is a significant step in improving the system efficiency, contributing to more effective energy utilization.

As shown in Figure 9, an increase in temperature resulted in an increase in thermal efficiency in the SOFC. With the operating temperature rising from 873 K to 1473 K, the thermal efficiency increased by 43.67%. At a constant current density of 7500 A/m², thermal efficiencies are 57.64% and 44.52% for operating temperatures of 1573 and 1073 K, respectively. Sinha et al. [58] analyzed the performance of a SOFC operating at high temperatures and fueled by biomass through simulation. According to these findings, an increase in thermal efficiency was observed with the rise in the operating temperature. For instance, at a temperature of 1150 K, the thermal efficiency was 66.2%, whereas it was determined to be 67.9% at an operating temperature of 1275 K.

The change in pore size in the SOFC was significantl, as shown in Figure 10. An increase in pore size linearly decreased the thermal efficiency. At a current density of  $12500 \text{ A/m}^2$ , doubling the pore size resulted in a 12.03% increase in thermal efficiency. Under a constant operating temperature in SOFC, the thermal efficiency was 56.59% with an  $8 \mu m$  pore size, while it decreased to 47.99% with a pore size of  $15 \mu m$ .

The variation in the thermal efficiency with the current density at elevated operating temperatures is presented in Table 3. As the temperature increased from 1273 K to 1673 K, the thermal efficiency decreased at low current densities (2500 A/m<sup>2</sup> – 7500 A/m<sup>2</sup>). The operating temperature at which maximum efficiency occurs changes as the current density increases. Therefore, material selection in SOFC design should consider the relationship between the operating temperature and current density.

## 4. CONCLUSIONS

- In this study, SOFC performance was evaluated under different operating temperatures (573-1673 K) and pore sizes (3-15 µm).
- The activation, ohmic and concentration losses were analyzed over cell potential, power density and thermal efficiency.
- It was observed that activation losses increased at low temperatures and negatively affected cell performance. Therefore, solutions should be developed to reduce the activation losses in systems that will operate at low temperatures.

- The concentration losses increased significantly as temperature increased; for example, a temperature increase of 200 K increased this loss by approximately 50% at constant current density.
- Reducing the pore diameter reduced activation losses; a 50% decrease in pore size provided a decrease in losses of 0.178 V.
- At a constant current density of 5000 A/m², a significant decrease in activation losses was observed as the operating temperature increased: the loss, which was 2.097 V at 573 K, decreased to 0.0053 V at 1673 K.
- However, a decreasing trend in thermal efficiency began at temperatures above 1273 K; for example, increasing the temperature from 1273 K to 1373 K led to a 2.70% efficiency loss.
- Exergy analyses should be performed to optimize cell design and operating conditions; thus, energy losses due to entropy production can be determined more accurately.
- This study clearly demonstrates the effects of different temperatures and pore structures on SOFC performance and paves the way for data-based improvement strategies for cell design.

#### Recommendations

Studies can be conducted on hybrid systems that will increase exergy efficiency in the energy production processes of SOFCs.

Studies can be conducted to develop catalysts that will reduce the activation energy for systems operating at low temperatures.

# **Funding**

No funds, grants, or other support was received.

**Declaration of interests:** The authors have no relevant financial or nonfinancial interests to disclose.

**Data access statement:** The data illustrated in the present study are available on a reasonable request from the authors.

## REFERENCES

1. Ringuedé, A., Hubert, S., Atwi, L., and Lair, V. "Prospects of hydrogen and its derivative as energy vector for electricity production at high temperature: Fuel cells and

- electrolysers" *Current Opinion in Electrochemistry*, **42**, pp. 101401 (2023). https://doi.org/10.1016/j.coelec.2023.101401
- 2. Nanadegani, F.S. and Sunden, B. "Review of exergy and energy analysis of fuel cells" *International Journal of Hydrogen Energy*, **48**, pp. 32875–32942 (2023). <a href="https://doi.org/10.1016/j.ijhydene.2023.05.052">https://doi.org/10.1016/j.ijhydene.2023.05.052</a>
- 3. Ilbas, M., Kumuk, B., Alemu, M.A., and Arslan, B. "Numerical investigation of a direct ammonia tubular solid oxide fuel cell in comparison with hydrogen" *International Journal of Hydrogen Energy*, **45**, pp. 35108–35117 (2020). <a href="https://doi.org/10.1016/j.ijhydene.2020.04.060">https://doi.org/10.1016/j.ijhydene.2020.04.060</a>
- 4. Ilbas, M. and Kumuk, B. "Numerical modelling of a cathode-supported solid oxide fuel cell (SOFC) in comparison with an electrolyte-supported model" *Journal of the Energy Institute*, **92**, pp. 682–692 (2019). https://doi.org/10.1016/j.joei.2018.03.004
- Cigdem, T., Onbilgin, S., Timurkutluk, B., and Panuk, I. "Effects of pore former type on mechanical and electrochemical performance of anode support microtubes in solid oxide fuel cells" *International Journal of Hydrogen Energy*, 47, pp. 11633–11643 (2022). <a href="https://doi.org/10.1016/j.ijhydene.2022.01.178">https://doi.org/10.1016/j.ijhydene.2022.01.178</a>
- 6. Wang, C., Fan, J., Xing, Y., and Guan, J. "Thermodynamics and electrochemical performance of co- and counter-flow planar solid oxide fuel cells under an adiabatic operation environment" *International Journal of Hydrogen Energy*, **50**(Part C), pp. 181-199 (2024). <a href="https://doi.org/10.1016/j.ijhydene.2023.08.094">https://doi.org/10.1016/j.ijhydene.2023.08.094</a>
- 7. Sahli, Y., Zitouni, B., and Ben-Moussa, H. "Solid oxide fuel cell thermodynamic study" *Çankaya University Journal of Science and Engineering*, **14**(2), pp. 134–151 (2017).
- 8. Cao, Y., Dhahad, H.A., Sun, Y.L., Haghghi, M.A., Delpisheh, M., Athari, H., and Farouk, N. "The role of input gas species to the cathode in the oxygen-ion conducting and proton conducting solid oxide fuel cells and their applications: Comparative 4E analysis" *International Journal of Hydrogen Energy*, **46**(37), pp. 19569–19589 (2021). https://doi.org/10.1016/j.ijhydene.2021.03.111
- 9. Afolabi, A.E., Sunday, K., Abdulkareem, A.S., Abdulsalam, Y.O., Kovo, A.S., and Oladijo, P. "Thermo-economic analysis of solid oxide fuel cell using human waste as a

- source of fuel" *Scientific African*, **14**, pp. e01024 (2021). https://doi.org/10.1016/j.sciaf.2021.e01024
- 10. Wang, J., Al-attab, K.A., and Yew Heng, T. "Techno-economic and thermodynamic analysis of solid oxide fuel cell combined heat and power integrated with biomass gasification and solar assisted carbon capture and energy utilization system" *Energy Conversion and Management*, **280**, pp. 116762 (2023). <a href="https://doi.org/10.1016/j.enconman.2023.116762">https://doi.org/10.1016/j.enconman.2023.116762</a>
- Kasaeian, A., Hadavi, H., Amirhaeri, Y., and Pourfayaz, F. "Thermodynamic analysis of a wood chips-based cycle integrated with solid oxide fuel cell" *Renewable Energy*, 195, pp. 1174–1193 (2022). <a href="https://doi.org/10.1016/j.renene.2022.06.101">https://doi.org/10.1016/j.renene.2022.06.101</a>
- Ghorbannejad, F., Khoshgoftar Manesh, M.H., Nemati, M., and Ghasemi, A. "A comprehensive exergoenvironment-emergoeconomic-emergoenvironment based analysis of hybrid steam biomass gasification and solid oxide fuel cell system for a multigeneration system" *Energy Reports*, 8, pp. 9057–9080 (2022). <a href="https://doi.org/10.1016/j.egyr.2022.07.001">https://doi.org/10.1016/j.egyr.2022.07.001</a>
- 13. Beigzadeh, M., Pourfayaz, F., Ghazvini, M., and Ahmadi, M.H. "Energy and exergy analyses of solid oxide fuel cell-gas turbine hybrid systems fed by different renewable biofuels: A comparative study" *Journal of Cleaner Production*, **280**, pp. 124383 (2021). <a href="https://doi.org/10.1016/j.jc/zpro.2020.124383">https://doi.org/10.1016/j.jc/zpro.2020.124383</a>
- 14. Selvam, K., Komatsu, Y., Sciazko, A., Kaneko, S., and Shikazono, N. "Thermodynamic analysis of 100% system fuel utilization solid oxide fuel cell (SOFC) system fueled with ammonia" *Energy Conversion and Management*, **249**, pp. 114839 (2021). <a href="https://doi.org/10.1016/j.enconman.2021.114839">https://doi.org/10.1016/j.enconman.2021.114839</a>
- 15. Sinha, A.A., Sanjay, Ansari, M.Z., Shukla, A.K., Verma, T.N., and Choudhary, T. "Thermodynamic assessment of biomass-fueled solid oxide fuel cell integrated gas turbine hybrid configuration" *Sustainable Energy Technologies and Assessments*, **57**, pp. 103242 (2023). <a href="https://doi.org/10.1016/j.seta.2023.103242">https://doi.org/10.1016/j.seta.2023.103242</a>
- 16. Ryu, B.R., Duong, P.A., and Kang, H. "Comparative analysis of the thermodynamic performances of solid oxide fuel cell–gas turbine integrated systems for marine vessels

- using ammonia and hydrogen as fuels" *International Journal of Naval Architecture and Ocean Engineering*, **15**, pp. 100524 (2023). <a href="https://doi.org/10.1016/j.ijnaoe.2023.100524">https://doi.org/10.1016/j.ijnaoe.2023.100524</a>
- 17. Pérez-Trujillo JP, Elizalde-Blancas F, Della Pietra M, Silva-Mosqueda, D.M., García Guendulain, J.M., and McPhail, S.J. "Thermoeconomic comparison of a molten carbonate fuel cell and a solid oxide fuel cell system coupled with a micro gas turbine as hybrid plants" *Energy Conversion and Management*, **276**, pp. 116533 (2023). <a href="https://doi.org/10.1016/j.enconman.2022.116533">https://doi.org/10.1016/j.enconman.2022.116533</a>
- 18. Alirahmi, S.M., Raisi, A., Ghasemi, B., and Nadooshan, A.A. "Comprehensive technoeconomic assessment and tri-objective optimization of an innovative integration of compressed air energy storage system and solid oxide fuel cell" *Renewable Energy*, **218**, pp. 119290 (2023). <a href="https://doi.org/10.1016/j.renene.2023.119290">https://doi.org/10.1016/j.renene.2023.119290</a>
- 19. Pirkandi, J., Penhani, H., and Maroufi, A. "Thermodynamic analysis of the performance of a hybrid system consisting of steam turbine, gas turbine and solid oxide fuel cell (SOFC-GT-ST)" *Energy Conversion and Management*, **213**, pp. 112816 (2020). <a href="https://doi.org/10.1016/j.enconman.2020.112816">https://doi.org/10.1016/j.enconman.2020.112816</a>
- 20. Kumuk, B., Atak, N.N., Dogan, B., Ozer, S., Demircioglu, P., and Bogrekci, I. "Numerical and thermodynamic analysis of the effect of operating temperature in methane-fueled SOFC" *Energies*, **17**(11), pp. 2603 (2024). https://doi.org/10.3390/en.7112603
- 21. Inac, S., Unverdi, S.O., and Midilli, A. "A parametric study on thermodynamic performance of a SOFC oriented hybrid energy system" *International Journal of Hydrogen Energy*, 44, pp. 10043–10058 (2019). <a href="https://doi.org/10.1016/j.ijhydene.2019.01.247">https://doi.org/10.1016/j.ijhydene.2019.01.247</a>
- 22. Akkaya, A.V., Sahin, B., and Erdem, H.H. "Thermodynamic model for exergetic performance of a tubular SOFC module" *Renewable Energy*, **34**, pp. 1863–1870 (2009). <a href="https://doi.org/10.1016/j.renene.2008.11.017">https://doi.org/10.1016/j.renene.2008.11.017</a>
- 23. Min, G., Park, Y.J., and Hong, J. "1D thermodynamic modeling for a solid oxide fuel cell stack and parametric study for its optimal operating conditions" *Energy Conversion and Management*, **209**, pp. 112614 (2020). https://doi.org/10.1016/j.enconman.2020.112614

- 24. Halis, S., Atak, N.N., and Doğan, B. "Investigation of the performance of cathode supported solid oxide fuel cell with energy and exergy analysis at different operating temperatures" *International Journal of Energy Studies*, **9**, pp. 21–42 (2024). https://doi.org/10.58559/ijes.1429413
- 25. Dogan, B. and Atak, N.N. "Exergy analysis in solid oxide fuel cells with different operating temperature and pore diameter" *Case Studies in Thermal Engineering*, **61**, pp. 104849 (2024). https://doi.org/10.1016/j.csite.2024.104849
- 26. Henke, M., Kallo, J., Friedrich, K.A., and Bessler, W.G. "Influence of pressurisation on SOFC performance and durability: A theoretical study" *Fuel Cells*, **11**, pp. 581–591 (2011). <a href="https://doi.org/10.1002/fuce.201000098">https://doi.org/10.1002/fuce.201000098</a>
- 27. Kumuk, B. and Ilbas, M. "Coal gas fuel utilization effects on electrolyte supported solide oxide fuel cell performance" *International Journal of Hydrogen Energy*, **46**, pp. 29523–29528 (2021). <a href="https://doi.org/10.1016/j.ijhydene.2020.19.179">https://doi.org/10.1016/j.ijhydene.2020.19.179</a>
- 28. Wang, Y., Zhan, R., Qin, Y., Zhang, G., Du, X., and Jiao, K. "Three-dimensional modeling of pressure effect on operating characteristics and performance of solid oxide fuel cell" *International Journal of Hydrogen Energy*, **43**, pp. 20059–20076 (2018). <a href="https://doi.org/10.1016/j.ijhydene.2018.09.025">https://doi.org/10.1016/j.ijhydene.2018.09.025</a>
- 29. Calise, F., Dentice d'Accadia, M., Palombo, A., and Vanoli, L. "Simulation and exergy analysis of a hybrid solid oxide fuel cell (SOFC)-gas turbine system" *Energy*, **31**, pp. 3278–3299 (2006). https://doi.org/10.1016/j.energy.2006.03.006
- 30. Suther, T., Fung, A.S., Koksal, M., and Zabihian, F. "Effects of operating and design parameters on the performance of a solid oxide fuel cell-gas turbine system" *International Journal of Energy Research*, **35**, pp. 616–632 (2011). <a href="https://doi.org/10.1002/er.1722">https://doi.org/10.1002/er.1722</a>
- 31. Yan, Z., He, A., Hara, S., and Shikazono, N. "Modeling of solid oxide fuel cell (SOFC) electrodes from fabrication to operation: Microstructure optimization via artificial neural networks and multi-objective genetic algorithms" *Energy Conversion and Management*, **198**, 111916 (2019). <a href="https://doi.org/10.1016/j.enconman.2019.111916">https://doi.org/10.1016/j.enconman.2019.111916</a>
- 32. Bertei, A., Nucci, B., and Nicolella, C. "Microstructural modeling for prediction of transport properties and electrochemical performance in SOFC composite electrodes"

- *Chemical Engineering Science*, **101**, pp. 175–190 (2013). https://doi.org/10.1016/j.ces.2013.06.032
- 33. Riazat, M., Baniassadi, M., Mazrouie, M., Tafazoli, M., and Moghimi Zand, M. "The effect of cathode porosity on solid oxide fuel cell performance" Energy Equipment and Systems, **3**(1), pp. 25–32 (2015). https://doi.org/10.22059/ees.2015.13908
- 34. Sinha, A.A., Sanjay, Ansari, M.Z., Shukla, A.K., and Choudhary, T. "Comprehensive review on integration strategies and numerical modeling of fuel cell hybrid system for power & heat production" *International Journal of Hydrogen Energy*, **48**, pp. 33669–33704 (2023). <a href="https://doi.org/10.1016/j.ijhydene.2023.05.097">https://doi.org/10.1016/j.ijhydene.2023.05.097</a>
- 35. Sinha AA, Choudhary T, Ansari, M. Z., Shukla, A.K., and Arabkoohsar, A. "Waste heat recovery and exergy-based comparison of a conventional and a novel fuel cell integrated gas turbine hybrid configuration" *Sustainable Energy Technologies and Assessments*, **57**, pp. 103256 (2023). <a href="https://doi.org/10.1016/j.seta.2023.103256">https://doi.org/10.1016/j.seta.2023.103256</a>
- 36. Sinha, A.A., Sanjay, Ansari, M.Z., Shukla, A.K., Verma, T.N., and Choudhary, T. "Thermodynamic assessment of biomass-fueled solid oxide fuel cell integrated gas turbine hybrid configuration" *Sustainable Energy Technologies and Assessments*, **57**, pp. 103242 (2023). <a href="https://doi.org/10.1016/j.set/1.2023.103242">https://doi.org/10.1016/j.set/1.2023.103242</a>
- 37. Sinha, A.A., Choudhary, T., Ansari, M.Z., and Sanjay. "Estimation of exergy-based sustainability index and performance evaluation of a novel intercooled hybrid gas turbine system" *International Journal of Hydrogen Energy*, **48**, pp. 8629–8644 (2023). <a href="https://doi.org/10.1016/j.ijhydene.2022.10.260">https://doi.org/10.1016/j.ijhydene.2022.10.260</a>
- 38. Choudhary, T. and Sanjay. "Computational analysis of IR-SOFC: Transient, thermal stress, carbon deposition and flow dependency" *International Journal of Hydrogen Energy*, **41**, pp. 10212–10227 (2016). <a href="https://doi.org/10.1016/j.ijhydene.2016.04.016">https://doi.org/10.1016/j.ijhydene.2016.04.016</a>
- 39. Sinha, A.A., Choudhary, T., Ansari, M.Z., and Shukla, A.K. "Energy, exergy, and sustainability a novel comparison of conventional gas turbine with fuel cell integrated hybrid power cycle" *International Journal of Hydrogen Energy*, **47**, pp. 34257–34272 (2022). https://doi.org/10.1016/j.ijhydene.2022.07.268

- 40. Choudhary, T. and Sanjay. "Novel and optimal integration of SOFC-ICGT hybrid cycle: Energy analysis and entropy generation minimization" *International Journal of Hydrogen Energy*, **42**, pp. 15597–15612 (2017). <a href="https://doi.org/10.1016/j.ijhydene.2017.04.277">https://doi.org/10.1016/j.ijhydene.2017.04.277</a>
- 41. Choudhary, T. and Sanjay. "Thermodynamic assessment of advanced SOFC-blade cooled gas turbine hybrid cycle" *International Journal of Hydrogen Energy*, **42**, pp. 10248–10263 (2017). <a href="https://doi.org/10.1016/j.ijhydene.2017.02.178">https://doi.org/10.1016/j.ijhydene.2017.02.178</a>
- 42. Choudhary, T. and Sanjay. "Computational analysis of IR-SOFC: Thermodynamic, electrochemical process and flow configuration dependency" *International Journal of Hydrogen Energy*, **41**, pp. 1259–1271 (2016). <a href="https://doi.org/10.1016/j.ijhydene.2015.10.098">https://doi.org/10.1016/j.ijhydene.2015.10.098</a>
- 43. Choudhary, T., Sahu, M., and Krishna, S. "Thermodynamic analysis of solid oxide fuel cell gas turbine hybrid system for aircraft power generation". *SAE Technical Paper*, **2017-01–2062**, 10 pages (2017). <a href="https://doi.org/10.4271/2017-01-2062">https://doi.org/10.4271/2017-01-2062</a>
- 44. Choudhary, T., Sahu, M.K., Kumari, A., and Mohapatra, A. "Thermodynamic Modeling of Blade Cooled Turboprop Engine Integrated to Solid Oxide Fuel Cell: A Concept" *SAE Technical Paper*, 2018-01–1308, 10 pages (2018). <a href="https://doi.org/10.4271/2018-01-1308">https://doi.org/10.4271/2018-01-1308</a>
- 45. Stambouli, A.B. and Traversa, E. "Solid oxide fuel cells (SOFCs): A review of an environmentally clean and efficient source of energy" *Renewable and Sustainable Energy Reviews*, 6, pp. 433–455 (2002). <a href="https://doi.org/10.1016/S1364-0321(02)00014-X">https://doi.org/10.1016/S1364-0321(02)00014-X</a>
- 46. Chan, S.H., Khor, K.A., and Xia, Z.T. "Complete polarization model of a solid oxide fuel cell and its sensitivity to the change of cell component thickness" *Journal of Power Sources*, 93, pp. 130–140 (2001). https://doi.org/10.1016/S0378-7753(00)00556-5
- 47. Ni, M., Leung, M.K.H., and Leung, D.Y.C. "Parametric study of solid oxide fuel cell performance" *Energy Conversion and Management*, **48**, pp. 1525–1535 (2007). <a href="https://doi.org/10.1016/j.enconman.2006.11.016">https://doi.org/10.1016/j.enconman.2006.11.016</a>
- 48. Three, C. "Fuel Cell Electrochemistry", *PEM fuel cells: theory and practice*, ed. Barbir, F., Academic press (2012). https://doi.org/10.1016/B978-012078142-3/50004-5

- 49. Chan, S.H. and Xia, Z.T. "Polarization effects in electrolyte/electrode-supported solid oxide fuel cells" *Journal of Applied Electrochemistry*, **32**, pp. 339–347 (2002). <a href="https://doi.org/10.1023/A:1015593326549">https://doi.org/10.1023/A:1015593326549</a>
- 50. Chan, S.H., Ho, H.K., and Tian, Y. "Multi-level modeling of SOFC-gas turbine hybrid system" *Journal of Power Sources*, **28**(8), pp. 889-900 (2003). <a href="https://doi.org/10.1016/S0360-3199(02)00160-X">https://doi.org/10.1016/S0360-3199(02)00160-X</a>
- 51. Ivers-Tiffée, E. and Virkar, A.V. "Electrode Polarisations", *High-temperature Solid Oxide Fuel Cells: Fundamentals, Design and Applications*, ed. Singhal, S.C. and Kendall, K., Elsevier Science, pp. 229–260 (2003). <a href="https://doi.org/10.1016/P978-185617387-2/50026-X">https://doi.org/10.1016/P978-185617387-2/50026-X</a>
- 52. Todd, B. and Young, J.B. "Thermodynamic and transport properties of gases for use in solid oxide fuel cell modelling" *Journal of Power Sources*, **110**(1), pp. 186-200 (2002). <a href="https://doi.org/10.1016/S0378-7753(02)00277-X">https://doi.org/10.1016/S0378-7753(02)00277-X</a>
- 53. Ferguson, J.R., Fiard, J.M., and Herbin, R. "Three-dimensional numerical simulation for various geometries of solid oxide fuel cells" *Journal of Power Sources*, **58**, pp. 109–122 (1996). <a href="https://doi.org/10.1016/0378-7753(95)02269-4">https://doi.org/10.1016/0378-7753(95)02269-4</a>
- 54. Chan, S.H., Ho, H.K., and Tian, Y. "Modelling of simple hybrid solid oxide fuel cell and gas turbine power plant" *Journal of Power Sources*, **109**, pp. 111–120 (2002). https://doi.org/10.1015/S0378-7753(02)00051-4
- 55. Singhal, S.C., "Advances in solid oxide fuel cell technology" *Solid State Ionics*, **135**, pp. 305–313 (2000). <a href="https://doi.org/10.1016/S0167-2738(00)00452-5">https://doi.org/10.1016/S0167-2738(00)00452-5</a>
- 56. Lin, B., Shi, Y., and Cai, N. "Numerical simulation of cell-to-cell performance variation within a syngas-fuelled planar solid oxide fuel cell stack" *Applied Thermal Engineering*, **114**, pp. 653–662 (2017). <a href="https://doi.org/10.1016/j.applthermaleng.2016.12.014">https://doi.org/10.1016/j.applthermaleng.2016.12.014</a>
- 57. Tsai, T. and Barnett, S.A. "Effect of LSM-YSZ cathode on thin-electrolyte solid oxide fuel cell performance" *Solid State Ionics*, **93**, pp. 207–217 (1997). https://doi.org/10.1016/s0167-2738(96)00524-3

58. Sinha, A.A., Saini, G., Sanjay, Shukla, A.K., Ansari, M.Z., Dwivedi, G., and Choudhary, T. "A novel comparison of energy-exergy, and sustainability analysis for biomass-fueled solid oxide fuel cell integrated gas turbine hybrid configuration" *Energy Conversion and Management*, **283**, pp. 116923 (2023). <a href="https://doi.org/10.1016/j.enconman.2023.116923">https://doi.org/10.1016/j.enconman.2023.116923</a>

Accepted by Scientia Tranica

# **List of Figures**

- Fig. 1 Basic structure and operating principle of a Solid Oxide Fuel Cell
- Fig. 2 Activation cell loss at different operating temperatures in a SOFC (  $D_p = 3 \mu m$ )
- Fig. 3 Activation cell loss at different pore sizes in a solid oxide fuel cell (T=1073 K)
- Fig. 4 Concentration cell loss at different operating temperatures in SOFC ( $D_p = 3 \mu m$ )
- Fig. 5 Cell voltage at different operating temperatures in SOFC ( $D_p = 3 \mu m$ )
- **Fig. 6** Cell voltage at different pore sizes in SOFC (T=1073 K)

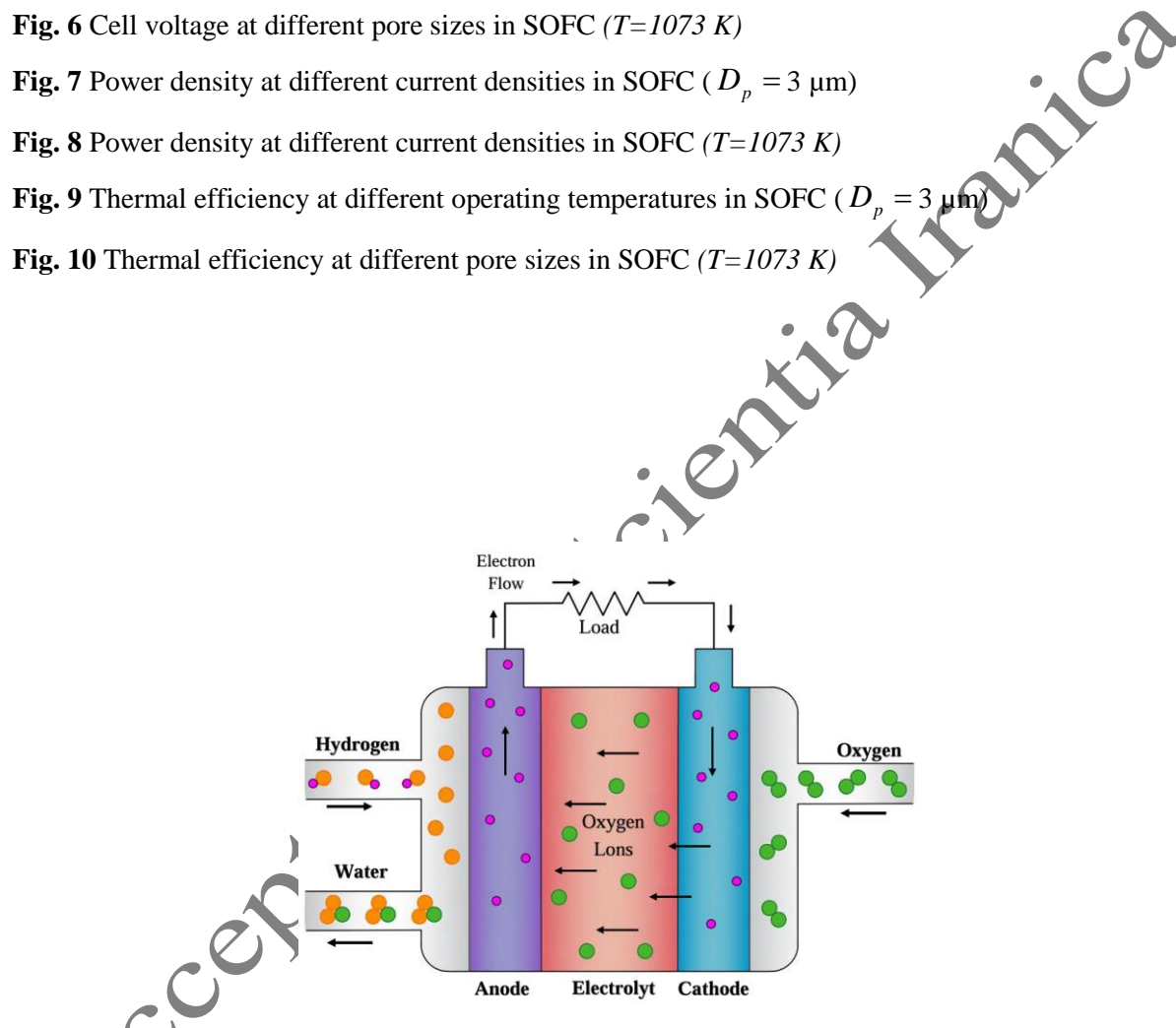


Fig. 1 Basic structure and operating principle of a Solid Oxide Fuel Cell

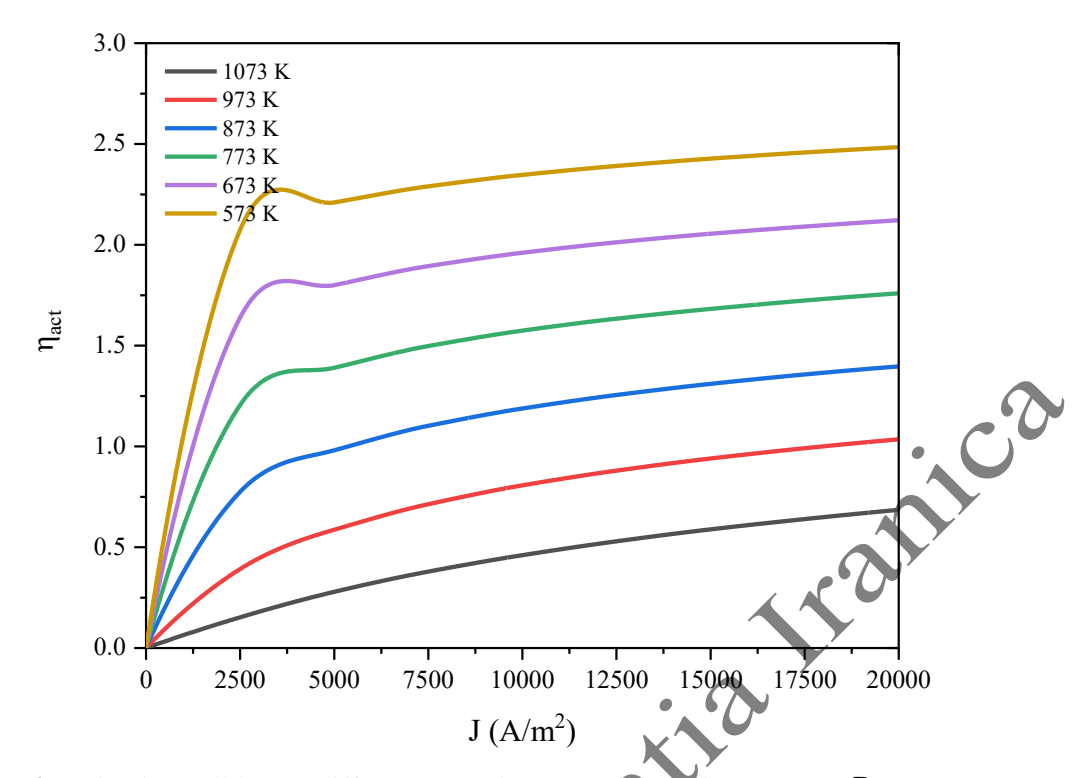


Fig. 2 Activation cell loss at different operating temperatures in a SOFC (  $D_p = 3 \mu m$ )

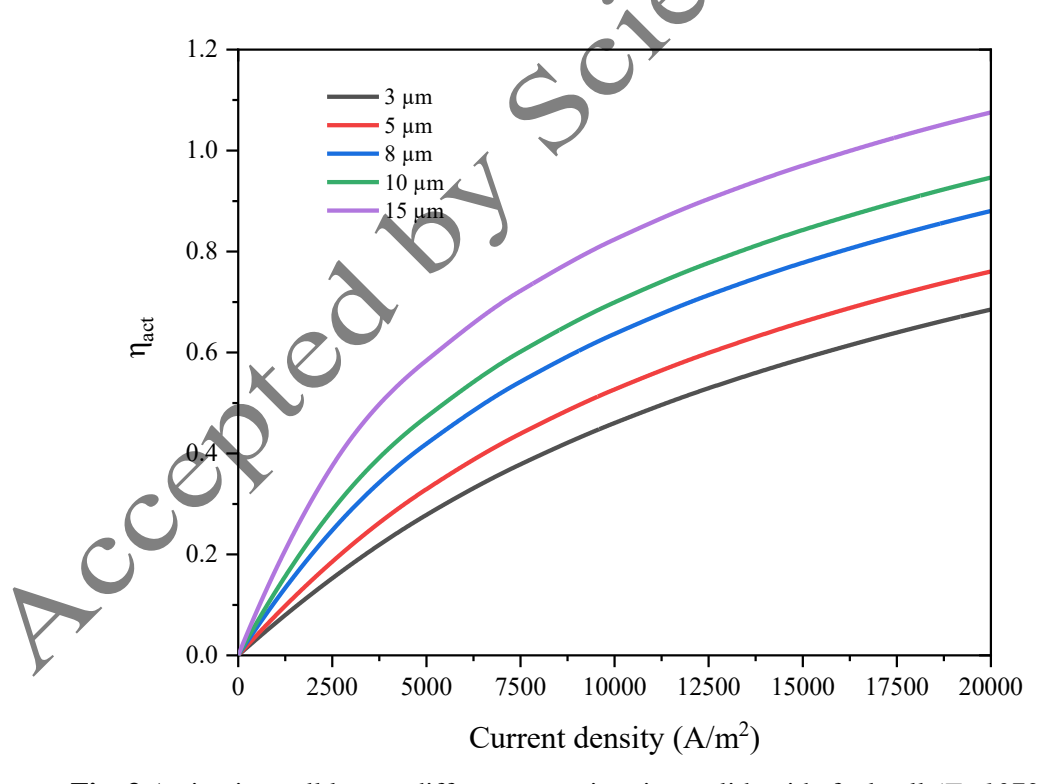


Fig. 3 Activation cell loss at different pore sizes in a solid oxide fuel cell  $(T=1073 \ K)$ 

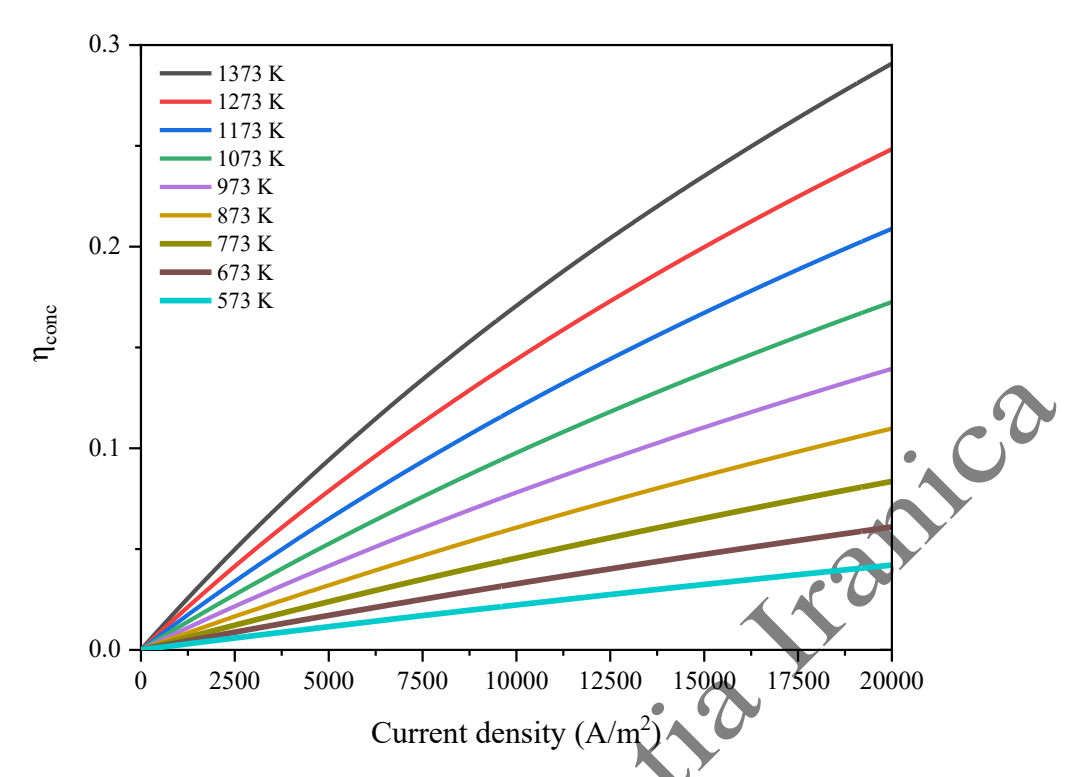


Fig. 4 Concentration cell loss at different operating temperatures in SOFC (  $D_p = 3 \ \mu m$ )

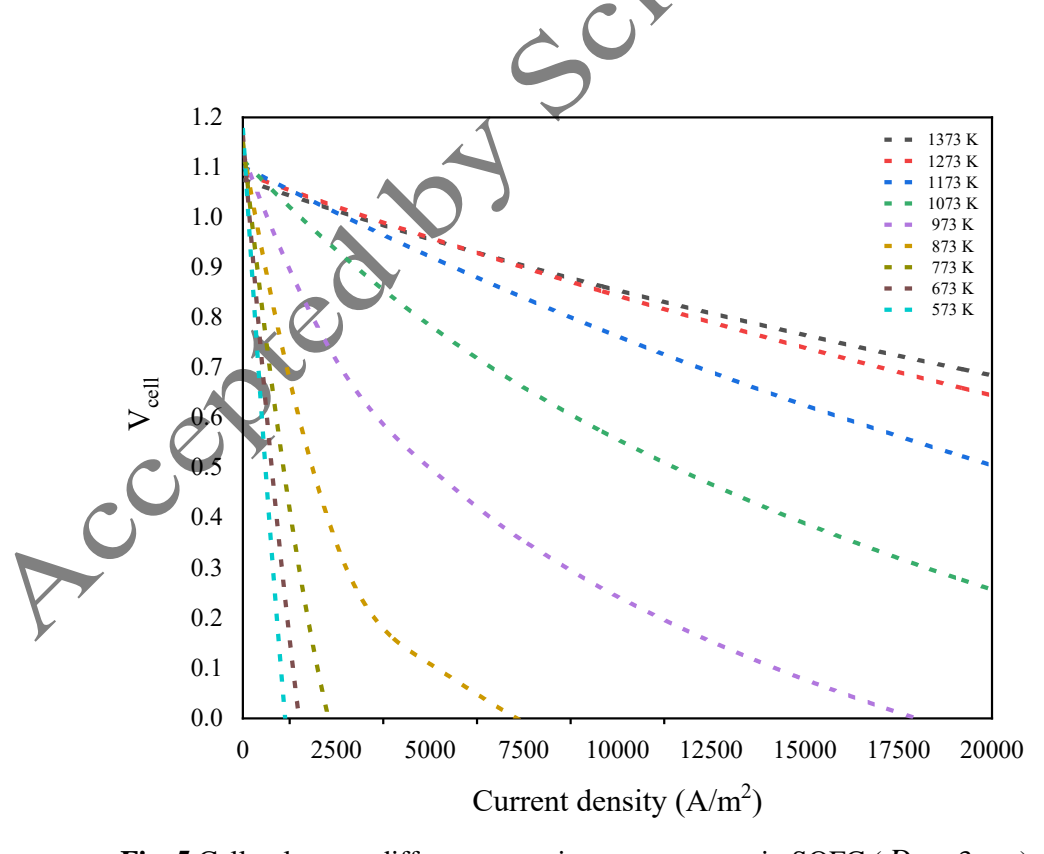


Fig. 5 Cell voltage at different operating temperatures in SOFC (  $D_{\scriptscriptstyle p}=3~\mu{\rm m})$ 

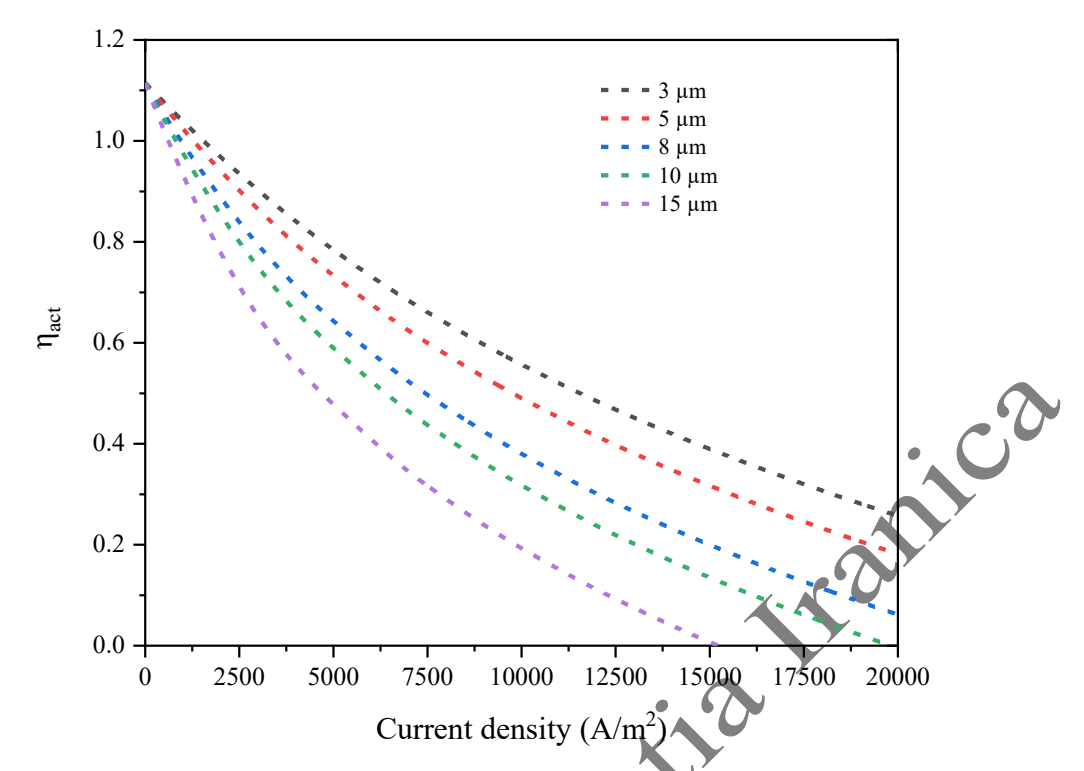


Fig. 6 Cell voltage at different pore sizes in SOFC (T=1073 K)

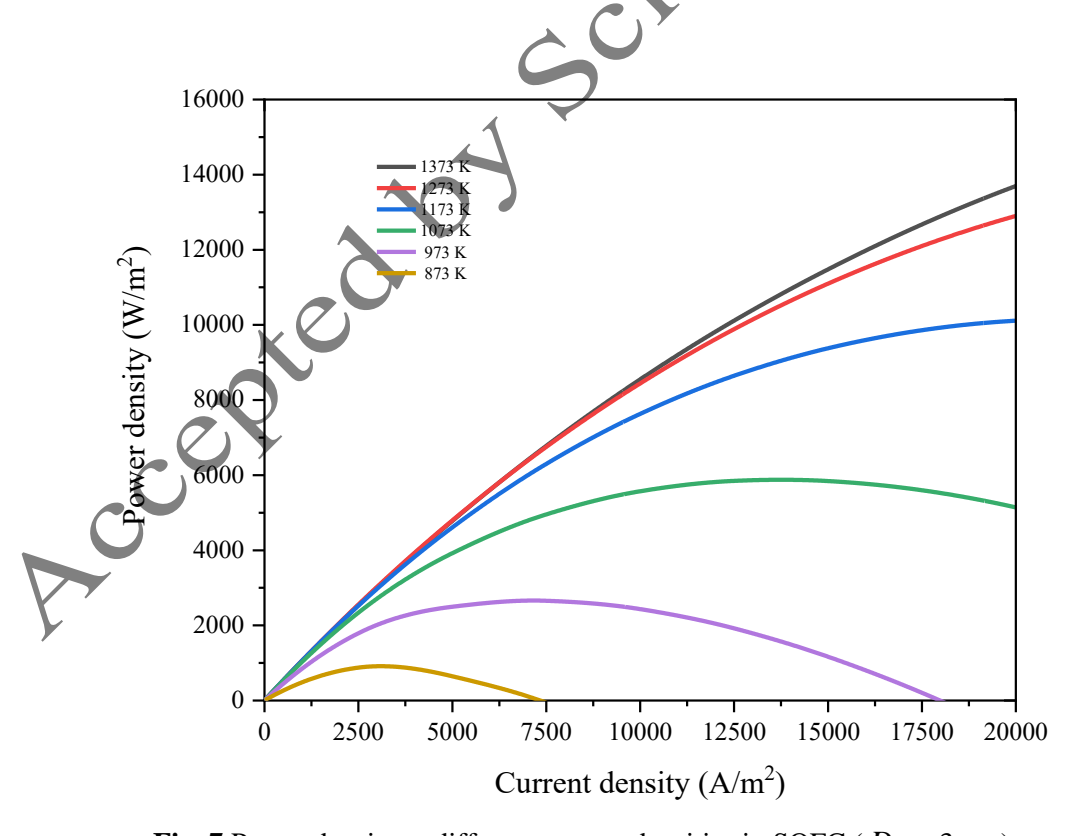


Fig. 7 Power density at different current densities in SOFC (  $D_{\it p}=3~\mu{\rm m})$ 

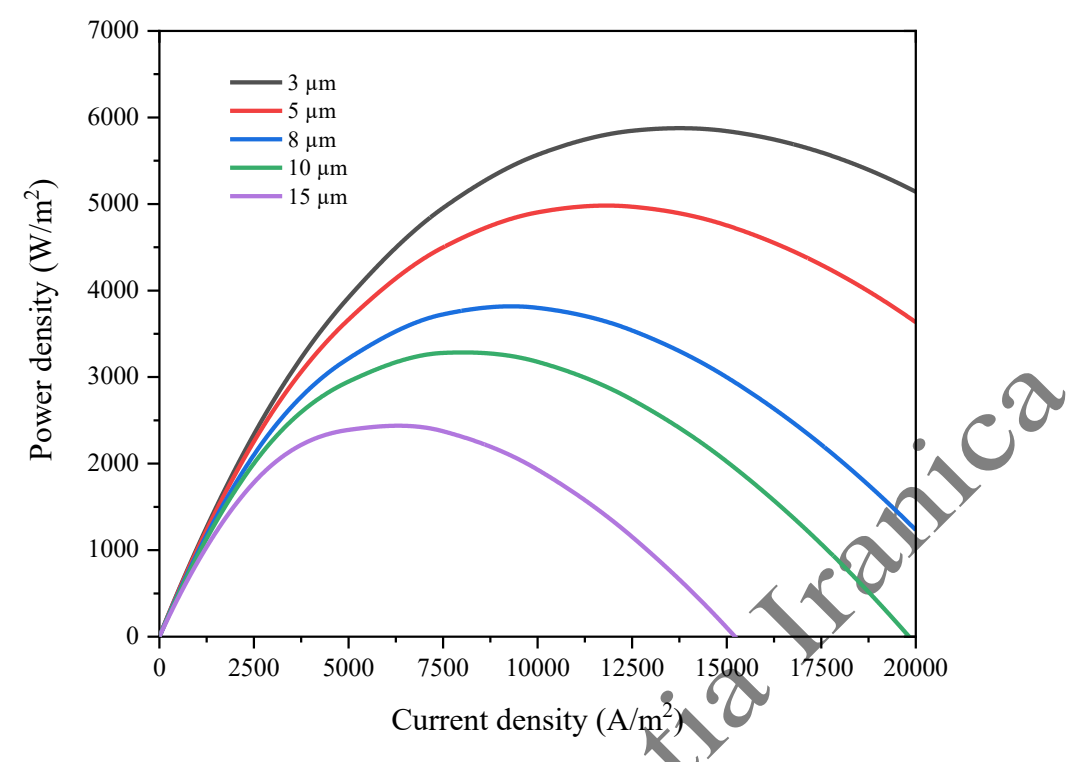


Fig. 8 Power density at different current densities in SOFC (T=1073~K)

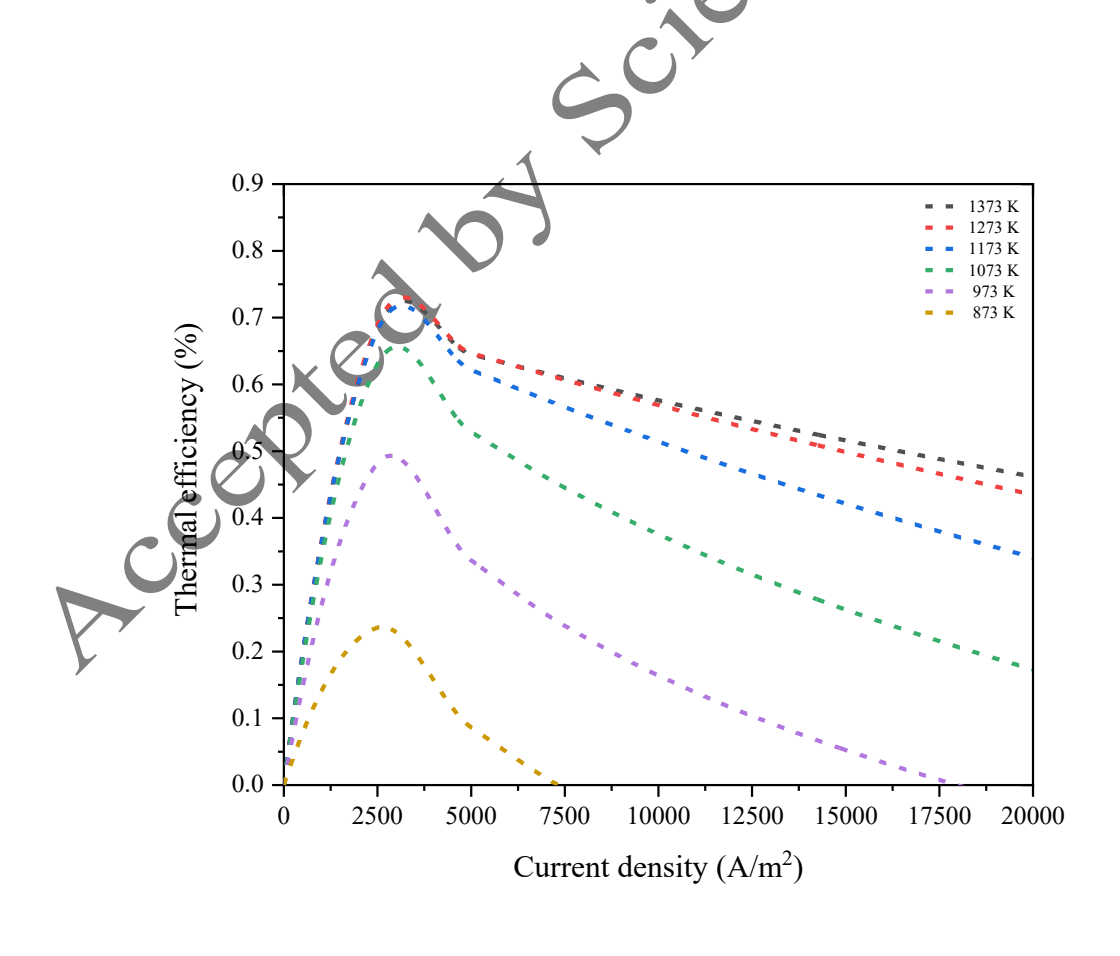


Fig. 9 Thermal efficiency at different operating temperatures in SOFC(  $D_p = 3 \mu m$ )

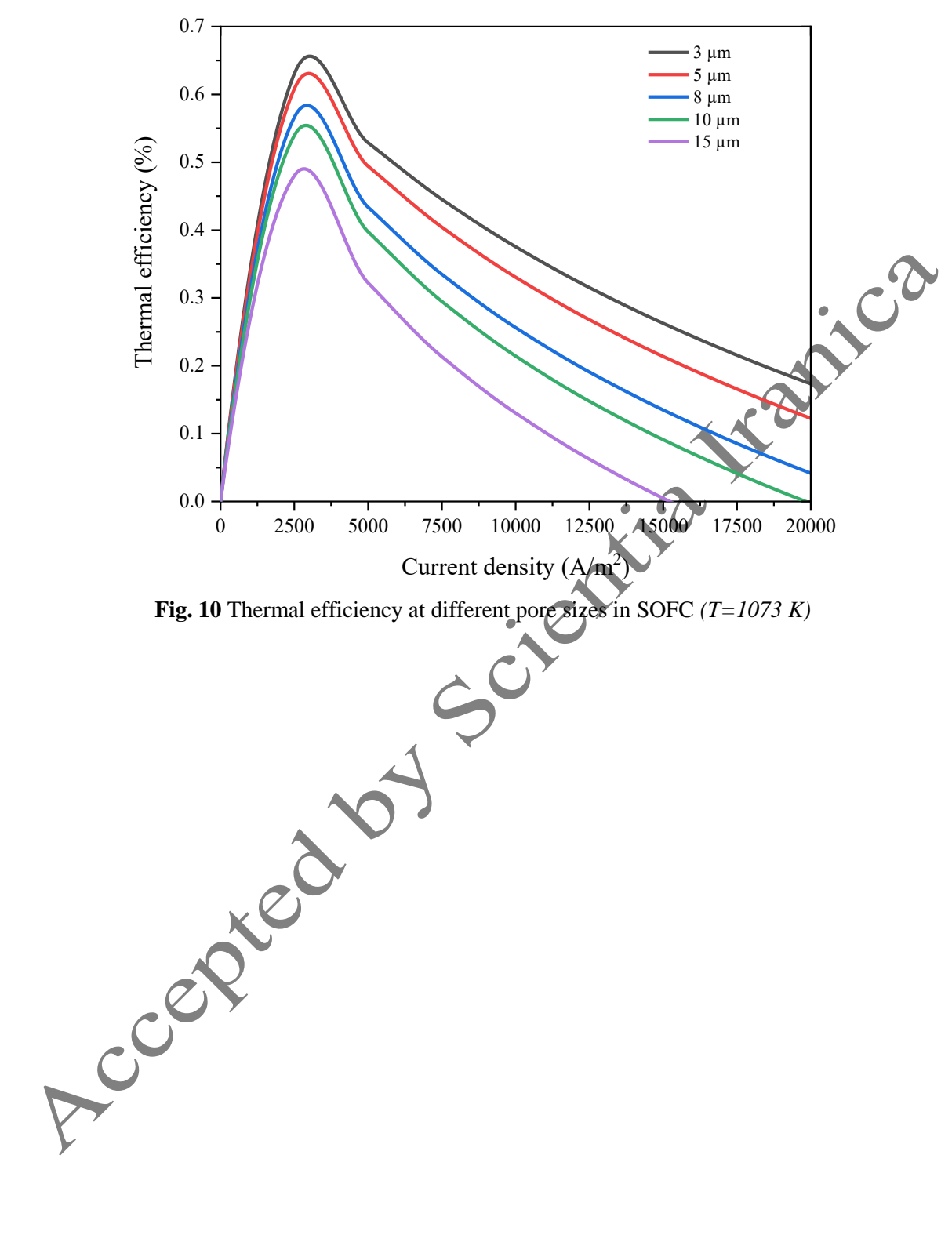


Fig. 10 Thermal efficiency at different pore sizes in SOFC (T=1073 K)

# **List of Tables**

Table 1. Parametric Values for Solid Oxide Fuel Cell

Table 2. Variation of activation losses at high temperatures

**Table 3.** Variation of thermal efficiencies at high temperatures

Table 1. Parametric Values for Solid Oxide Fuel Cell

Parameter	Unit	Value
Faraday constant, F	[C/mol]	96485
Universal gas constant, R	[J/mol K]	8.3145
Operating temperature, T	[K]	573-1673
Operating pressure, P	[bar]	1
Activation energy for anode, $E_{act,a}$	[J/mol]	$1.344 \times 10^{10}$
Activation energy for cathode, $E_{cc,c}$	[J/mol]	2.051×10 <sup>9</sup>
Anode porosity, <i>n</i>	-	0.48
Anode tortuosity, $\xi$	-	5.4
Average length of grain contact, X	-	0.7
Average pore radius, $D_p$	[m]	$3-15\times10^{-6}$
Average grain size, $D_s$	[m]	$1.5 \times 10^{-6}$
Anode thickness, $d_a$	[m]	$1000 \times 10^{-6}$
Cathode thickness, $d_c$	[m]	20×10 <sup>-6</sup>
Electrolyte thickness, L	[m]	8×10 <sup>-6</sup>
Active cell area, A	[m]	0.01

**Table 2.** Variation of activation losses at high temperatures

J (A/m <sup>2</sup> )	1273 K	1373 K	1473 K	1573 K	1673				
	$\eta_{act}\left(V\right)$	$\eta_{act}\left(V\right)$	$\eta_{act}\left(V\right)$	$\eta_{act}\left(V\right)$	$\eta_{act}\left(V\right)$				
2500	0.0254	0.0126	0.0069	0.0041	0.0026				
5000	0.0507	0.0252	0.0139	0.0083	0.0053				
7500	0.0759	0.0378	0.0208	0.0125	0.0080				
10000	0.1007	0.0504	0.0278	0.0166	0.0106				
12500	0.1251	0.0630	0.0348	0.0208	0.0133				
15000	0.1491	0.0755	0.0417	0.0250	0.0160				
17500	0.1726	0.0879	0.0486	0.0291	0.0186				
20000	0.1955	0.1003	0.0556	0.0333	0.0213	,			
Table 3. Variation of thermal efficiencies at high temperatures									
J (A/m <sup>2</sup> )	1273 K	1373 K	1473 K	1573 K	1673 K	ı			
2500	68.88%	68.32%	67.21%	65.85%	64.35%	ı			

Table 3. Variation of thermal efficiencies at high temperatures

(	J (A/m <sup>2</sup> )	1273 K	1373 K	1473 K	1573 K	1673 K
	2500	68.88%	68.32%	67.21%	65.85%	64.35%
	5000	64.66%	64.47%	63.24%	61.52%	59.52%
	7500	60.67%	60.92%	59.64%	57.64%	55.26%
	10000	56.89%	57.62%	56.33%	54.13%	51.44%
	12500	53.30%	54.51%	53.28%	50.92%	47.97%
	15000	49.87%	51.59%	50.43%	47.96%	44.80%
	17500	46.60%	48.81%	47.76%	45.21%	41.88%
_	20000	43.47%	46.16%	45.25%	42.64%	39.16%

## **Biographies**

**Berre KÜMÜK** is an Assistant Professor at İskenderun Technical University, Department of Automotive Technologies. She received her M.Sc. (2018) and Ph.D. (2022) degrees from Gazi University, Ankara. Her research interests include mathematical modeling, characterization of fuel cells and electrolyzers, and thermodynamic analysis of integrated energy systems. She has contributed as a co-author to numerous scientific publications on fuel cells and renewable energy systems.

Nisa Nur ATAK is currently in her fourth year at Gazi University, Department of Energy Systems Engineering, where she started her education in 2020. Nurdil Teknik Soğutma has worked as an intern at the Ministry of Energy and Natural Resources and Electricity Generation Corporation (EÜAŞ). During her undergraduate education, she successfully completed the project titled "Using Renewable Energy Resources in Greenhouse Activities in Central Anatolia Region", which was accepted with in the scope of TÜBİTAK 2209-A University Students Research Projects Support Program. She is currently conducting a study supported by GAZİ BAP (Scientific Research Projects Coordination Unit) with the project title "Exergy of Using TiO<sub>2</sub> Nano Fluid Additives to Diesel Fusel Oil Fuel Blends in Internal Combustion Engines". She has many papers presented in symposiums, three book chapters and articles published in international journals.

**Battal DOĞAN** graduated from Kırıkkale University, Faculty of Engineering, Department of Mechanical Engineering in 2000. He completed his master's degree in 2002 and his doctorate in 2010 at Kırıkkale University, Institute of Science, Department of Mechanical Engineering. He worked as a Research Assistant and Lecturer at Kırıkkale University. He served as Engineer, Head of Department and Deputy General Manager at the Ministry of Transport. He has been working as a Lecturer in Gazi University, Faculty of Technology, Department of Energy Systems Engineering since July 20, 2021. He has many articles published in national and international journals, papers presented at symposiums and two books.

Murat Kadir YEŞİLYURT is an Associate Professor at the Department of Mechanical Engineering, Yozgat Bozok University, Yozgat, Türkiye. He received his BSc degree in the Department of Mechanical Engineering, Faculty of Engineering, Çukurova University, Adana, Türkiye in 2011. He received his MSc and PhD degrees in Mechanical Engineering from Kırıkkale University in 2013 and Bozok University in 2017, respectively. His main research interest includes internal combustion engines, alternative fuels, combustion, energy, and exergy analyses in thermal systems. He has published over 60 scientific papers in international and national journals/conferences. He has also done many scientific research projects.

Accepted by Scientia Iranica